Received: 26 June 2023 | Revised: 1 August 2023 | Accepted: 2 August 2023

DOI: 10.1002/pamm.202300043

RESEARCH ARTICLE

Ductile damage and failure of thin sheet metals: New biaxial experiments and numerical simulations

Steffen Gerke | **Fabuer R. Valencia** | **Michael Brünig**

Institut für Mechanik und Statik, Universität der Bundeswehr München, Neubiberg, Germany

Correspondence
Steffen Gerke, Institut für Mechanik und Statik, Universität der Bundeswehr München, Werner-Heisenberg-Weg 39, 85579 Neubiberg, Germany.
Email: steffen.gerke@unibw.de

Funding information
Deutsche Forschungsgemeinschaft, Grant/Award Number: 455960756

Abstract

The paper deals with the ductile damage and failure behavior of thin sheet metals under proportional biaxial loading paths. A newly designed specimen is presented and an experimental series with different loading ratios is performed. Corresponding numerical simulations including plastic anisotropy reflect the stress state and enable the interpretation of the different damage mechanisms. Due to fabrication issues the specimen geometry for this class of materials has to get by without notches in thickness direction and consequently the new specimens pre-define the localization by a series of holes. The strain fields at the specimen surface are evaluated by digital image correlation and the fracture surface is analyzed by scanning electron microscopy. The experimental and numerical methods described here provide a possibility for the targeted investigation of the ductile damage behavior of thin sheet metals under proportional loading.

1 | INTRODUCTION

Nowadays structural components have to fulfill economic, ecological as well as structural demands. Specially in lightweight applications such as in aeronautical and automotive industry high quality metallic alloys have been developed and are employed. During production and usage the structures are often loaded differently leading to a big variety of stress states whereat failure has to be avoided. Consequently, detailed analysis of irreversible deformations as well as of damage and fracture behavior of these alloys is mandatory to understand and to optimize the manufacturing processes and to assure safety during the life cycle.

For the systematic investigation of the stress-state-dependent material behavior of sheet metals it is necessary to carefully select or design the appropriate specimens. In literature a big variety of specimens has been presented, see for instance [1–4] and [5] for an overview. Of special interest in this context are biaxial geometries which can be applied for different loading scenarios. The X0-specimen and the H-specimen [6] have been successfully used to investigate the damage and failure behavior of sheets with moderate thickness under proportional and non-proportional loading [7, 8]. In the context focused on here, the geometry of the H-specimen is of special interest. It is characterized by a central opening and four notched regions where damage and failure occurrence is predefined. The notches are aligned in parallel to one loading axis allowing an almost direct relation between applied load and resulting stress state. Unfortunately, for the thin sheets considered here, it is no longer possible to insert notches in thickness direction to determine the region of high strains

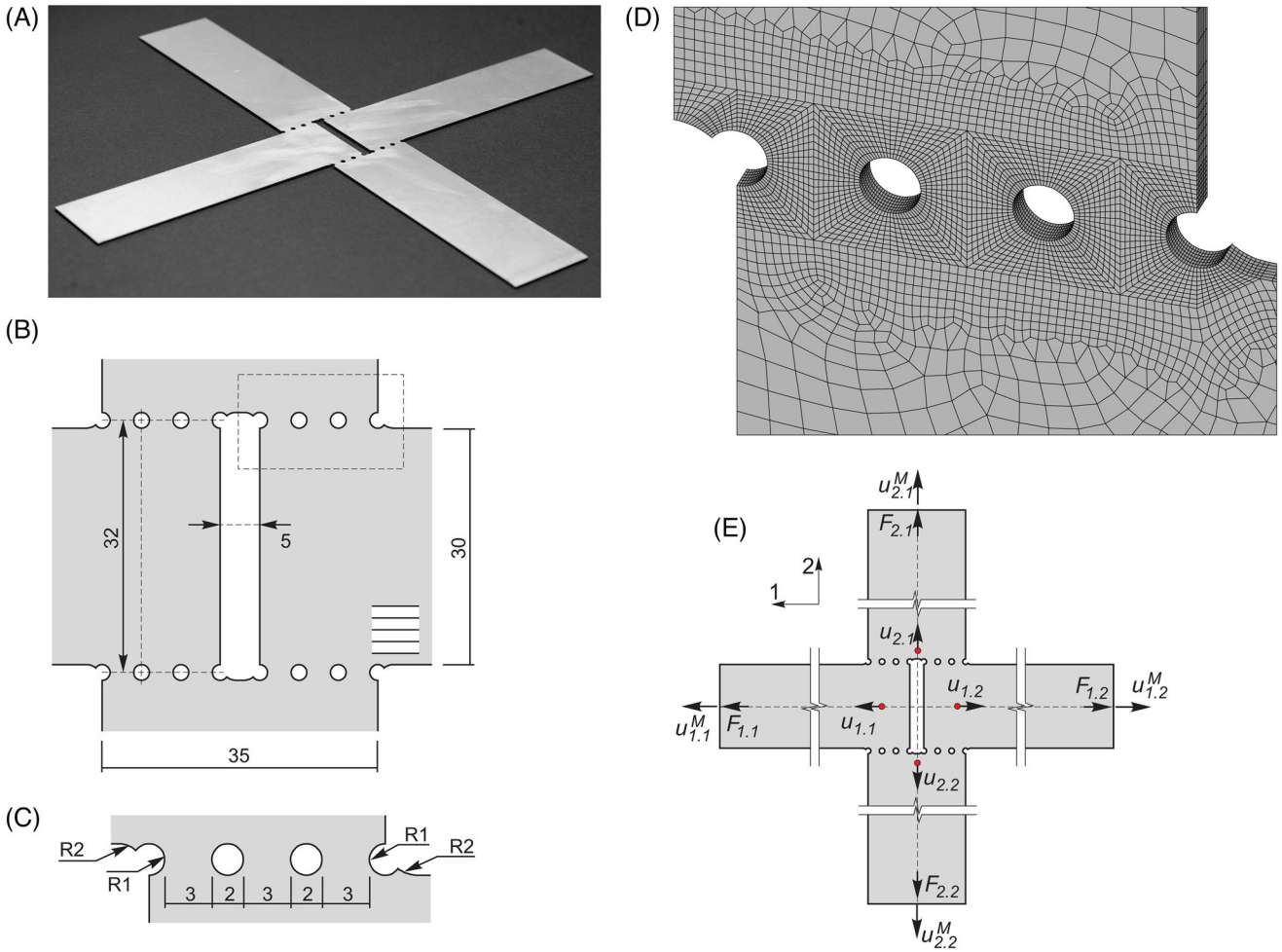

FIGURE 1 Specimen geometry and notation: (A) image, (B) central part, (C) detail, (D) mesh, and (E) notation; all measures in [mm].

and failure. Consequently, the H-specimens cannot be used without significant modifications and a new approach to the design of biaxial specimens for thin sheet metal has to be found. Furthermore, material anisotropy plays an important role for most thin sheets. In [9] the possibility is presented to manufacture geometrically equal biaxial test specimens in different directions to the main axes of material anisotropy and to test them under equal proportional loading conditions.

2 | SPECIMEN DESIGN, MATERIAL, AND SETUP

Standard dog-bone tensile specimens are characterized by an almost homogeneous stress and strain field before occurrence of necking. In contrast, the region of elevated strains and fracture is directly determined for in-sheet-plane-notched tensile specimens [1, 2, 10] whereat a smaller notch radius leads to a more concentrated region of elevated strains [11]. A similar effect can be achieved with central hole tensile specimens [12]. Consequently, the insertion of holes in combination with lateral notches represents a suitable possibility to predefine the area with increased inelastic strains. Based on these considerations and based on the H-specimen the design shown in Figure 1A–C is newly proposed here. The external dimensions are 240 by 240 mm and the radius of the holes and notches introduced is 1.0 mm. The geometry presented in Figure 1A–C is characterized by a central opening leading to four weakened areas. Each of these areas consists of three connectors separated by holes. Each of the three remaining connectors has a cross-sectional area of 3.0 mm^2, and a cross-sectional area of 9.0 mm^2 remains per connector area, making the specimens sufficiently robust to handle. The biaxial tests are conducted on a LFM-BIAX machine provided by Walter+Bai, Löhningen, Switzerland. It is equipped with four individually controllable electro-mechanical cylinders with maximum loads of ±20 kN where the biaxial specimens are

TABLE 1 Chemical decomposition based on a cast analysis aluminum alloy AA6016-T4, 1 mm.

Si	Fe	Cu	Mn	Mg	Cr	Zn	Ti
1.200	0.238	0.079	0.138	0.384	0.019	0.014	0.020

TABLE 2 Lankford coefficients for the aluminum alloy AA6016-T4, 1 mm.

r_{0°	r_{45°	r_{90°
0.6827	0.4369	0.6333

clamped by means of jaws. Details on the testing routine can be found in [7]. The four force signals ($F_{i.j}$, see Figure 1E) and machine displacements ($u^{\mathrm{M}}_{i.j}$, see Figure 1E) are transmitted to the stereo digital image correlation (DIC) system provided by Limess, Krefeld, Germany (Dantec), where the machine data is stored together with that from the DIC system. The corresponding DIC evaluations have a resolution of 65 px/mm while the selected subset size is 33 px (square) with an overlap of 11 px. In addition, the averaged forces per axis and an adequate relative displacement measure (Figure 1E) for data interpretation are introduced

$$F_i = \frac{F_{i.1} + F_{i.2}}{2} \qquad \text{and} \qquad \Delta u_{\mathrm{ref.i}} = u_{i.1} + u_{i.2}. \tag{1}$$

The applied elastic-plastic phenomenological material model is based on experimental observations on the macro-scale [9, 13]. The elastic behavior is assumed to be isotropic and governed by Hooke's law whereas the anisotropic plastic behavior for thin metal sheets assuming plane stress conditions is characterized by the Hill [14] yield condition

$$f^{\mathrm{pl}} = \left\{ \frac{1}{2}\left[(G+H)\bar{T}_x^2 - 2H\bar{T}_x\bar{T}_y + (F+H)\bar{T}_y^2 \right] + N\bar{T}_{xy}^2 \right\}^{\frac{1}{2}} - \bar{c} = 0. \tag{2}$$

In Equation (2), $\bar{T}_i$ represent the respective components of the Kirchhoff stress tensor, F, G, H, and N are the anisotropy parameters identified by different uni-axial experiments and $\bar{c}$ denotes the equivalent stress measure which in the present approach is taken to be the tensile yield stress of the uni-axial specimen cut in rolling direction (RD), $\bar{c} = \bar{c}_x$. In the analysis the evolution of the equivalent stress measure is modeled by the Voce law

$$\bar{c} = c_o + R_o \epsilon^{\mathrm{pl}} + R_\infty \left(1 - e^{-b\,\epsilon^{\mathrm{pl}}} \right) \tag{3}$$

where c_o represents the initial yield stress, R_o and R_∞ are hardening moduli, b denotes the hardening exponent and ϵ^{pl} means the equivalent plastic strain measure. Furthermore, plastic strains occurring during the loading process are determined by the associated flow rule given in components for the here applied plane stress case

$$\dot{H}_x^{\mathrm{pl}} = \dot{\lambda}\left[(G+H)\bar{T}_x - H\bar{T}_y \right], \quad \dot{H}_y^{\mathrm{pl}} = \dot{\lambda}\left[(F+H)\bar{T}_y - H\bar{T}_x \right] \quad \text{and} \quad \dot{H}_{xy}^{\mathrm{pl}} = \dot{\lambda} N \bar{T}_{xy} \tag{4}$$

where $\dot{\lambda}$ is the scalar-valued plastic equivalent strain rate measure describing the amount of plastic strains. In addition, assuming isochoric plastic deformation the plastic strain rate in thickness direction is given by

$$\dot{H}_z^{\mathrm{pl}} = -\left(\dot{H}_x^{\mathrm{pl}} + \dot{H}_y^{\mathrm{pl}} \right) = \dot{\lambda}\left(G\bar{T}_x + F\bar{T}_y \right). \tag{5}$$

A detailed representation of the material model as well as a discussion on material parameter determination is given in [9, 13].

For the experimental series presented here the aluminum alloy AA6016-T4 of 1 mm thickness and with chemical composition listed in Table 1 is used. Experiments with uni-axially loaded specimens cut in RD, diagonal direction (DD), and transverse direction (TD) have been performed. The DIC measurement of the three-dimensional displacement and strain fields provide the strain increments which can be used to determine the r-values (Lankford coefficients) given in Table 2.

TABLE 3 Material parameters of the aluminum alloy AA6016-T4, 1 mm.

K[MPa]	E[MPa]	c_0[MPa]	R_0[MPa]	R_∞[MPa]	b[−]	F[−]	G[−]	H[−]	L[−]	M[−]	N[−]
57500	69000	155	260	130	16	1.362	1.189	0.811	3	3	2.327

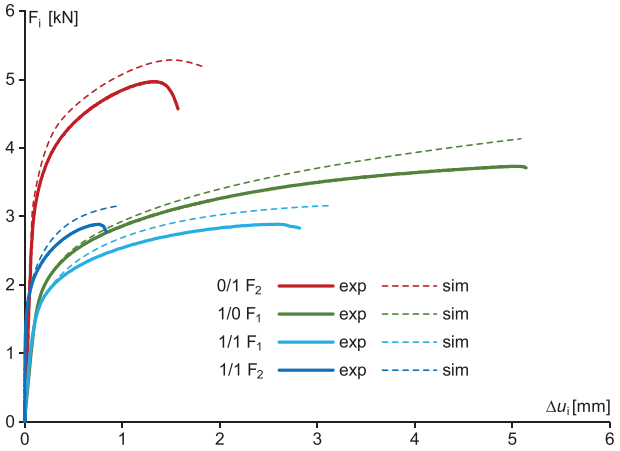

FIGURE 2 Experimental (exp) and numerically calculated (sim) load-displacement-curves.

Corresponding numerical analysis has been carried out with the finite element program ANSYS in connection with the material model presented above. A quarter of the specimens is divided into eight-node-elements of type SOLID185 using symmetry boundary conditions to reduce numerical costs resulting into 24 084 elements, see Figure 1E. Refinement of the finite element mesh has been realized in the perforated parts to accurately predict the expected stress states and its gradients. The respective displacements are applied to the nodes at the end faces and are iterated to meet the corresponding load ratio. Out-of-plane movements are neglected by zero displacements in this direction of the nodes in the symmetry planes at the end surfaces. All material parameters needed for the simulation of the aluminum alloy AA6016-T4 are given in Table 3.

3 | EXPERIMENTAL AND NUMERICAL RESULTS

The experimental series presented here consists of three load cases with proportional loading $F_1/F_2 = 0/1$, $1/0$ and $1/1$. Variations on the material orientation have not been realized and the RD coincides with the direction of axis 1, see Figure 1A,D where the RD is indicated by parallel lines. Intuitively the geometry can be accessed: By loading only axis 2 (vertical, Figure 1D, 0/1) the weakened, perforated areas of the specimen are mainly tension loaded, which is augmented by geometry of the holes. In contrast, if only axis 1 (horizontal, Figure 1D, 1/0) is loaded this part of the specimen is predominately shear loaded whereas slight tension can occur due to the offset caused by the perforations. And the third load case 1/1 can be seen as an combination of the previously discussed one. Besides this concrete engineering approach, a detailed analysis of the experimental and numerical results can depict new insights with respect to the inelastic behavior leading to failure.

The global deformation behavior under different loading conditions is reflected by the load-displacement diagrams shown in Figure 2. Corresponding loads F_i and the relative displacements u_i are calculated as given in Equation 1 and on the numerical side the forces and relative displacements have been doubled due to the numerical model reduction. Under $F_1/F_2 = 0/1$ loading the highest force overall ($F_2 = 4.9$ kN) at a relative displacement $\Delta u_2 = 1.45$ mm is reached. 1/0 reaches a maximum of $F_1 = 3.65$ kN at $\Delta u_1 = 5.2$ mm. Consequently 1/0 loading results in a significantly more ductile behavior. Under combined loading 1/1 the maximum loads $F_1 = F_2 = 2.85$ kN are reached at $\Delta u_1 = 2,55$ mm and $\Delta u_2 = 0.8$ mm. Compared with the uni-axial load cases both maximum force as well as the corresponding displacements are reduced, but as combined loading is applied, the results due reflect this combination. The numerical curves can reproduce the elastic-plastic behavior of the experiments qualitatively well but they slightly overestimate the forces. Here it has to

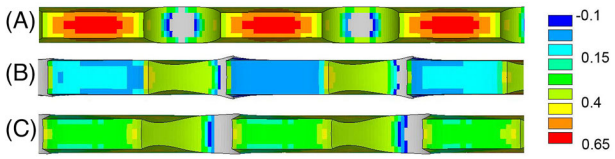

FIGURE 3 Numerically calculated stress triaxiality η: (A) $F_1/F_2 = 0/1$, (B) $1/0$, and (C) $1/1$.

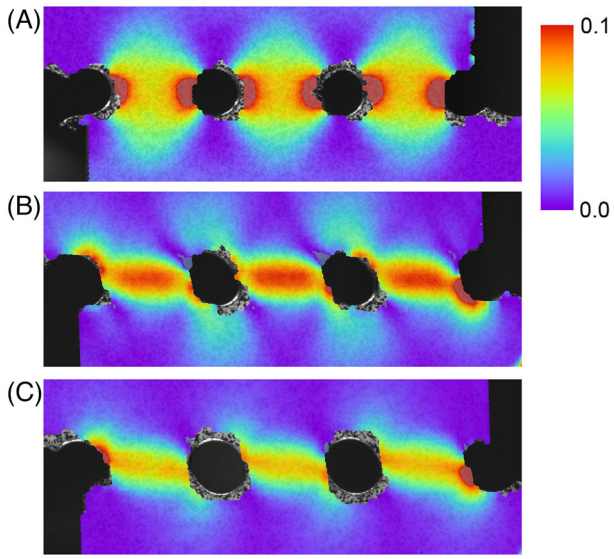

FIGURE 4 First principal strain at approximately 0.1 maximum: (A) $F_1/F_2 = 0/1$, (B) $1/0$, and (C) $1/1$.

be mentioned, that the material parameters have been fitted as discussed above based on uni-axially loaded experiments and have not been altered afterwards. Furthermore, the anisotropic ductile damage behavior leading to softening is not reflected in the constitutive formulation so far.

The stress triaxiality $\eta = \bar{\sigma}_m/\bar{\sigma}_{eq}$ with $\bar{\sigma}_m$ indicating the mean stress and $\bar{\sigma}_{eq}$ the equivalent von Mises stress is an important quantity related to the damage mechanisms. Positive stress triaxiality values of $1/3$ (tension dominated) and above lead to void growth and values close to zero (shear dominated) lead to micro shear cracks as dominant damage mechanism. Figure 3 indicates the numerically calculated stress triaxialities in the three connectors at $2/3$ of the maximum displacement. For loading in axis 2 ($F_1/F_2 = 0/1$, Figure 3A) values of $\eta = 0.6$ are reached at the center of the connectors and they reduce toward the perforations to 0.38. Under axis 1 loading ($1/0$, (b)) values between 0.05 and 0.12 with a homogeneous distribution and for combined loading ($1/1$, (c)) values around 0.28 are calculated. Consequently, the numerical results confirm the initially intuitively interpreted setup. Overall it can be noted, that the three connectors behave very similarly among each other which can be seen as a positive indicator of the specimen geometry.

Figure 4 displays the first principal strain of the three connectors marked in Figure 1B at 0.1 maximum value. Under tension loading ($F_1/F_2 = 0/1$, (a)) maximum values occur at the perforations and towards the center of the connectors the first principal strains reduce significantly to half of the values (here 0.05). This deformation behavior is typical for notched tension specimens, see for instance [15]. These strain gradients are less pronounced for the load cases $1/0$ and $1/1$ where a band of elevated strains develops with characteristic inclination and width depending on the loading. At this point it is important to mention, that the deformation behavior of the load cases with significant loading in axis 1 ($1/0$ and $1/1$) is comparable to the one observed in one dimensional shear experiments with two shear connectors [12]. For all three load cases again the three connectors behave very similarly among each other.

The final failure of the specimen typically occurs by fracture of two weakened areas, that is, six connectors fail nearly simultaneously. Figure 5 displays fractured specimens of the here discussed load cases. For the tension dominated load case $F_1/F_2 = 0/1$ (5(a)) the fracture direction is nearly parallel to axis 1 and reflects the strains displayed in Figure 4A. The deformation of the weakened zones at fracture is characterized by elongations in loading direction leading to elliptical

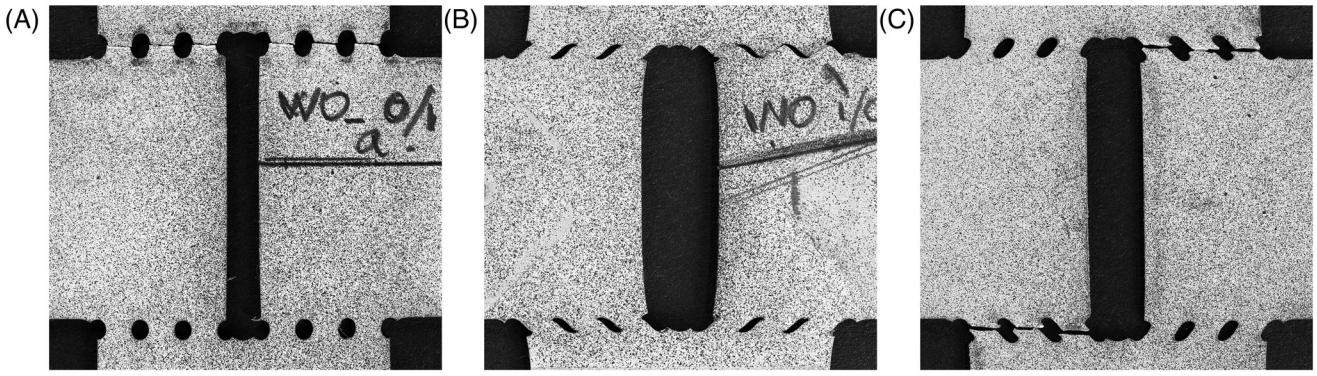

FIGURE 5 Fractured specimens: (A) $F_1/F_2 = 0/1$, (B) $1/0$, and (C) $1/1$.

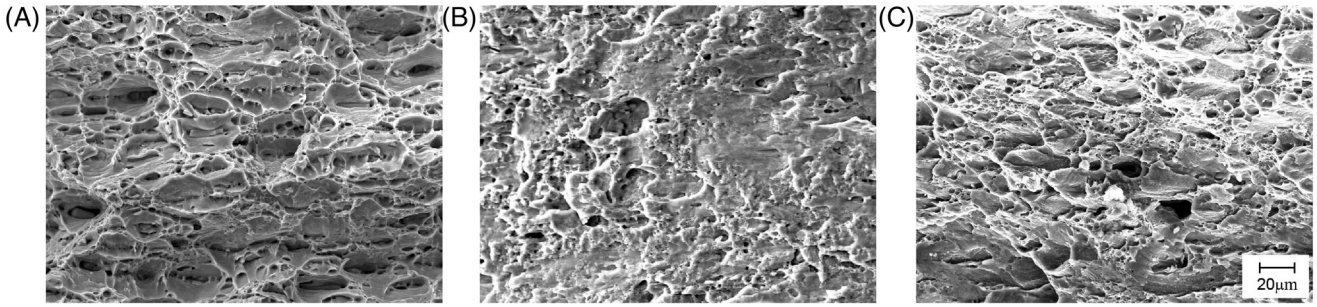

FIGURE 6 SEM images: (A) $F_1/F_2 = 0/1$, (B) $1/0$, and (C) $1/1$. SEM, scanning electron microscopy.

perforations. Overall, the fractured specimen (0/1) indicates moderate strains and reflects the moderate displacements indicated in Figure 2. The fractured specimen under shear dominated loading (1/0, (b)) depicts high strains and high rotations of the connector material whereas only one weakened area fractured (top right). In the deformation process principal strains of 0.1 are reached early (Figure 4B) and in continuation more elevated strains employ leading to a fracture line inclined towards the center of the specimen. The elevated strain level is also reflected in the high relative displacements before fracture, see Figure 2. Under combined loading (1/1, (c)) the fracture line is slightly inclined to the outside reflecting the strains displayed in Figure 4C. In general, the deformation and fracture behavior under combined loading (1/1) can be seen as a combination of the uni-axial load cases (0/1 and 1/0).

Figure 6 displays images of the fracture surfaces taken by scanning electron microscopy (SEM) for each load case in the center of the middle connector. The pre-fracture stress state characterized by the stress triaxiality η (Figure 3) can be well related to the damage mechanism that resulted in the crack [16]. For the load case 0/1 significant void growth before fracture, see Figure 6A, is displayed which relates to tension dominated mechanisms as indicated by high stress triaxialities, see Figure 3A. Under 1/0 loading smeared shear dimples indicate shear stresses superimposed by slight tension (Figure 6B) caused by small positive stress triaxialities as shown in Figure 3B. Under combined loading significant void growth with shear influence is indicated. This can be seen as a combination of the previously discussed uni-axial load cases and reflects the present stress state (Figure 3C).

Altogether, the series of tests presented here with newly introduced specimens for thin sheets demonstrates very well the possibilities of biaxial tests for the investigation of ductile damage behavior. Due to the different loads applied, different damage mechanisms could be specifically generated and a superposition of these is also well accessible.

4 | CONCLUSIONS

The results presented in this publication with a newly designed specimens for thin sheet metal indicate the reliable starting point of a comprehensive series of experiments which has to be extended over a wide range of stress states. These results

can be used to identify the damage behavior of plastic anisotropic metals. The main findings and conclusions of this paper are:

- A new specimen geometry for thin sheet metals has been motivated and proposed. In its design, notches in thickness direction are avoided and consequently the fabrication is enabled for thin sheet metals and overall simplified.
- The newly presented specimen for thin sheets allows the systematic investigation of the material behavior of plastically anisotropic materials including damage and failure.
- The experimental series presented here is comprehensive due to the direct connection between loading and resulting stress state. Furthermore, the presented results (SEM images, Figure 6) indicate the different damage mechanisms.
- The tree connectors of one weakened section behave very similarly during the deformation process until fracture occurrence and the application of the proposed geometry seems reasonable.

In the future the experimental series has to be extended to further loading conditions including the for thin sheets challenging compressive loading in one axis. Furthermore, the material orientation has to be included, that is, specimens have to be fabricated in different inclinations to the RD. The consideration of the material orientation will lead to significantly more extensive test programs. Biaxial testing facilitates different loading scenarios and consequently target-oriented non-proportional loading is possible and facilitates the study of history dependent loading. On the material modeling side the anisotropic plastic description has to be combined with ductile damage and fracture to enable simulations in this range.

ACKNOWLEDGMENTS

The authors gratefully acknowledge financial support of the Deutsche Forschungsgemeinschaft (DFG, German Research Foundation) – project number 455960756. Furthermore, the SEM images of the fracture surfaces presented in this paper have been performed at the Institut für Werkstoffe des Bauwesens at the Universität der Bundeswehr München and the special support of Wolfgang Saur is gratefully acknowledged.

Open access funding enabled and organized by Projekt DEAL.

ORCID

Steffen Gerke https://orcid.org/0000-0003-2261-3855

REFERENCES

1. Bai, Y., & Wierzbicki, T. (2008). A new model of metal plasticity and fracture with pressure and Lode dependence. *International Journal of Plasticity*, *24*(6), 1071–1096.
2. Brünig, M., Chyra, O., Albrecht, D., Driemeier, L., & Alves, M. (2008). A ductile damage criterion at various stress triaxialities. *International Journal of Plasticity*, *24*(10), 1731–1755.
3. Kuwabara, T. (2007). Advances in experiments on metal sheets and tubes in support of constitutive modeling and forming simulations. *International Journal of Plasticity*, *23*(3), 385–419.
4. Dunand, M., & Mohr, D. (2011). Optimized butterfly specimen for the fracture testing of sheet materials under combined normal and shear loading. *Engineering Fracture Mechanics*, *78*(17), 2919–2934.
5. Gerke, S., Zistl, M., & Brünig, M. (2020). Experiments and numerical simulation of damage and fracture of the X0-specimen under non-proportional loading paths. *Engineering Fracture Mechanics*, *224*, 106795.
6. Gerke, S., Adulyasak, P., & Brünig, M. (2017). New biaxially loaded specimens for the analysis of damage and fracture in sheet metals. *International Journal of Solids and Structures*, *110-111*, 209–218.
7. Gerke, S., Zistl, M., Bhardwaj, A., & Brünig, M. (2019). Experiments with the X0-specimen on the effect of non-proportional loading paths on damage and fracture mechanisms in aluminum alloys. *International Journal of Solids and Structures*, *163*, 157–169.
8. Brünig, M., Gerke, S., & Zistl, M. (2019). Experiments and numerical simulations with the H-specimen on damage and fracture of ductile metals under non-proportional loading paths. *Engineering Fracture Mechanics*, *217*, 106531.
9. Brünig, M., Koirala, S., & Gerke, S. (2022). Analysis of damage and failure in anisotropic ductile metals based on biaxial experiments with the H-specimen. *Experimental Mechanics*, *62*, 183–197.
10. Gao, X., Wang, T., & Kim, J. (2005). On ductile fracture initiation toughness: Effects of void volume fraction, void shape and void distribution. *International Journal of Solids and Structures*, *42*(18-19), 5097–5117.
11. Driemeier, L., Brünig, M., Micheli, G., & Alves, M. (2010). Experiments on stress-triaxiality dependence of material behavior of aluminum alloys. *Mechanics of Materials*, *42*(2), 207–217.
12. Roth, C. C., & Mohr, D. (2016). Ductile fracture experiments with locally proportional loading histories. *International Journal of Plasticity*, *79*, 328–354.

13. Brünig, M., Gerke, S., & Koirala, S. (2021). Biaxial experiments and numerical analysis on stress-state-dependent damage and failure behavior of the anisotropic aluminum alloy EN AW-2017A. *Metals*, *11*(8), 1214.
14. Hill, R. (1948). A theory of the yielding and plastic flow of anisotropic metals. *Proceedings of the Royal Society of London. Series A. Mathematical and Physical Sciences*, *193*(1033), 281–297.
15. Bonora, N., Gentile, D., Pirondi, A., & Newaz, G. (2005). Ductile damage evolution under triaxial state of stress: Theory and experiments. *International Journal of Plasticity*, *21*(5), 981–1007.
16. Brünig, M., Gerke, S., & Hagenbrock, V. (2013). Micro-mechanical studies on the effect of the stress triaxiality and the Lode parameter on ductile damage. *International Journal of Plasticity*, *50*, 49–65.

How to cite this article: Gerke, S., Valencia, F. R., & Brünig, M. (2023). Ductile damage and failure of thin sheet metals: New biaxial experiments and numerical simulations. *Proceedings in Applied Mathematics and Mechanics*, *23,* e202300043. https://doi.org/10.1002/pamm.202300043